De novo generation of a transmissible spongiform encephalopathy by mouse transgenesis

Christina J. Sigurdson[a,1], K. Peter R. Nilsson[a], Simone Hornemann[b], Mathias Heikenwalder[a], Giuseppe Manco[a], Petra Schwarz[a], David Ott[a], Thomas Rülicke[c], Pawel P. Liberski[d], Christian Julius[a], Jeppe Falsig[a], Lothar Stitz[e], Kurt Wüthrich[b,f], and Adriano Aguzzi[a,2]

[a]UniversitätsSpital Zürich, Institute of Neuropathology, CH-8091 Zürich, Switzerland; [b]Institut für Molekularbiologie und Biophysik, ETH Zürich, CH-8093 Zürich, Switzerland; [c]Institute of Laboratory Animal Science and Research Center Biomodels Austria, University of Veterinary Medicine Vienna, A-1210 Vienna, Austria; [d]Department of Molecular Pathology and Neuropathology, Medical University Lodz, Pl 92-216, Lodz, Poland; [e]Friedrich-Loeffler-Institute, Institute of Immunology, 72076 Tübingen, Germany; and [f]Department of Molecular Biology and Skaggs Institute for Chemical Biology, The Scripps Research Institute, La Jolla, CA 92037

Communicated by Charles Weissmann, Scripps Florida, Jupiter, FL, October 23, 2008 (received for review August 4, 2008)

Most transmissible spongiform encephalopathies arise either spontaneously or by infection. Mutations of *PRNP*, which encodes the prion protein, PrP, segregate with phenotypically similar diseases. Here we report that moderate overexpression in transgenic mice of mPrP(170N,174T), a mouse PrP with two point mutations that subtly affect the structure of its globular domain, causes a fully penetrant lethal spongiform encephalopathy with cerebral PrP plaques. This genetic disease was reproduced with 100% attack rate by intracerebral inoculation of brain homogenate to *tga20* mice overexpressing WT PrP, and from the latter to WT mice, but not to PrP-deficient mice. Upon successive transmissions, the incubation periods decreased and PrP became more protease-resistant, indicating the presence of a strain barrier that was gradually overcome by repeated passaging. This shows that expression of a subtly altered prion protein, with known 3D structure, efficiently generates a prion disease.

amyloid | neurodegeneration | prion | species barrier | transgenic mice

Prions cause fatal neurodegenerative disorders termed transmissible spongiform encephalopathies (TSEs). The prion contains a misfolded and aggregated form, PrP^{Sc}, of the host cellular prion protein, PrP^{C} (1). Accordingly, $Prnp^{o/o}$ mice that lack the gene encoding PrP^{C} resist prion infection (2).

Human familial TSEs co-segregate with more than 20 mutations in the prion gene, *PRNP* (3–5). Some of these genetic diseases have been transmitted to primates or mice (6, 7). De novo production of infectious prions from *PRNP* with point mutations would represent a useful tool for elucidating the origin of prion infectivity in genetic TSEs. Transgenic mice expressing *Prnp* with point mutations, insertions, or deletions develop a spectrum of neurological diseases with clinical or histological features reminiscent of TSEs (8–11). However, de novo infectivity was claimed only for mice expressing $Prnp^{P101L}$, which mimics the Gerstmann–Sträussler–Scheinker-associated P102L point mutation of human *PRNP*. $Prnp^{P101L}$ mice were reported to transmit disease to nine of 148 (6%) hamsters (10) but not to mice expressing WT PrP (10, 12). Transgenic mice expressing high amounts of $Prnp^{P101L}$ were thought to transmit spongiform encephalopathy to mice expressing lower amounts of $Prnp^{P101L}$ (10, 12), yet further studies led to the re-interpretation of this phenomenon as disease acceleration rather than bona fide transmission (13). A further set of transgenic mice expressing $Prnp^{P101L}$ produced by targeted gene substitution did not develop a neurological disease (6).

Mammalian PrP^{C} consists of a flexibly disordered N-terminal segment and a globular C-terminal domain containing three α-helices and two short antiparallel β-strands (14). However, the loop linking the β2 strand with the α2 helix displays remarkable species-specific variations. The β2—α2 loop region of human, cattle, mouse, dog, and cat is disordered, whereas that of elk is precisely defined (15–18). This feature is caused by S170N/N174T substitutions (numbering according to ref. 19), as documented by studies of variant mouse PrP containing the two residues 170N and 174T (16).

To probe the pathogenic impact of the well structured loop observed by NMR (16), we expressed in vivo a murine *Prnp* mini-gene with the S170N and N174T exchanges. This mouse-elk PrP chimeric molecule, henceforth termed RL-PrP for "rigid loop PrP," accumulated in detergent-resistant membranes similarly to WT PrP. Surprisingly, RL-PrP transgenic mice developed a transmissible spongiform encephalopathy. The novel variety of prions produced by RL-PrP transgenic mice was distinct from other commonly used laboratory prion strains.

Results

mPrP(170N,174T) Expression in Transgenic Mice. Two point mutations, G → A and A → C, were introduced at nucleotide positions 506 and 518 of the *Prnp* ORF within the pHGPrP vector (20), causing it to encode RL-PrP [supporting information (SI) Fig. S1 *A*, *B*, *E* and *F*] embedded in a "half-genomic" *Prnp* minigene. Linearized constructs were microinjected into B6;129S5-$Prnp^{+/o}$ zygotic pronuclei and founders were bred to B6;129S5-$Prnp^{o/o}$ mice. Transgene copy numbers and brain protein expression levels were determined by quantitative Southern and Western blotting of hemizygous mice. Line *tg*1020 mice had ≈45 copies of the transgene (Fig. S1*C*) and expressed approximately two- to threefold WT PrP levels in brain (Fig. S1*D*). PrP expression in *tg*1020 mice was higher than in most corresponding WT tissues (Fig. S2). In the *tg*1020 mouse line, RL-PrP^{C} glycosylation patterns, presence in detergent-resistant membranes, and functionality as shown by rescue of Shmerling disease (Fig. S2) (11) were indistinguishable from those of PrP^{C} (Figs. S2 and S3).

Spontaneous Neurodegenerative Disease in *tg*1020 Mice. Clinical monitoring of aging *tg*1020 mice revealed a progressive neurological illness with ataxia, hind limb paresis, weight loss, lethargy, kyphosis, and occasionally pruritus, which slowly progressed in severity over 1 to 3 months (Fig. 1*A*). Onset occurred at 145 to 637 days of age (50% incidence by 364 days; n = 47; Fig. 1*B*). Footprint tracks

Author contributions: C.J.S., M.H., K.W., and A.A. designed research; C.J.S., K.P.R.N., S.H., M.H., G.M., P.S., D.O., T.R., P.P.L., C.J., J.F., and L.S. performed research; K.P.R.N. contributed new reagents/analytic tools; C.J.S., K.P.R.N., S.H., M.H., P.P.L., C.J., J.F., K.W., and A.A. analyzed data; and C.J.S., S.H., K.W., and A.A. wrote the paper.

Conflict of interest statement: K.P.R.N. has interest in BioChromix AB (Linköping, Sweden), which owns some intellectual property in the amyloid binding luminescent conjugated polymers, PTAA and PTMI, described. The other authors declare no conflict of interest.

See Commentary on page 10.

[1]Present address: Department of Pathology, University of California at San Diego, La Jolla, CA 92037.

[2]To whom correspondence should be addressed. E-mail: adriano.aguzzi@usz.ch.

This article contains supporting information online at www.pnas.org/cgi/content/full/0810680105/DCSupplemental.

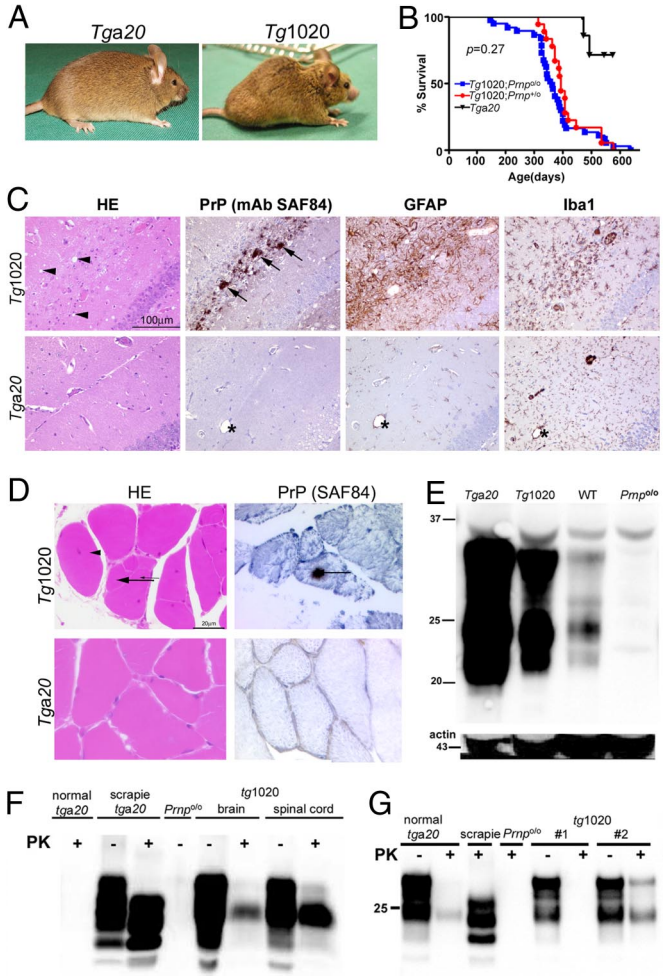

Fig. 1. RL-PrP mice (*tg*1020) develop a lethal neurologic disease with lesions in brain and muscle. (*A*) Clinically healthy *tga20* mouse (*Left*) and *tg*1020 mouse showing kyphosis and paraparesis, with hind legs tucked under the body. (*B*) Survival plots of *tg*1020;*Prnp*$^{o/o}$, *tg*1020;*Prnp*$^{+/o}$, and *tga20* mice. *Tga20* mice showed the typical life expectancy of C57BL/6 mice (41) held in specified pathogen-free environments, whereas *tg*1020;*Prnp*$^{o/o}$ and *tg*1020;*Prnp*$^{+/o}$ mice displayed median survival times of 363 and 394 days, respectively. (*C*) Hippocampi of *tg*1020 and *tga20* mice. Arrows indicate spongiform change. Linear arrays of PrP aggregates were accompanied by severe gliosis and microglial activation, as detected by antibodies to PrP, GFAP, and Iba1, respectively. Asterisk indicates a small vessel in a section of a *tga20* brain. (*D*) Myopathy in *tg*1020 but not *tga20* mice, with centralized nuclei (arrowhead), split fibers (arrow), and hypervariable fiber calibers. PrP immunostains show deposits (arrow) in affected *tg*1020 muscles. (*E*) Muscle PrP expression in *tg*1020 mice is higher than in WT but lower than in *tga20* mice. (*F*) PK-resistant PrP in *tg*1020 brains revealed by immunoblotting. There is no shift in the electrophoretic mobility, indicating lack of amino terminal cleavage of PrP. (*G*) Some young *tg*1020 mice (60 days old) also show PK-resistant PrP (mouse 2). Mouse 1 does not have PK-resistant PrP.

demonstrated circling movements of *tg*1020 mice indicative of ataxia (Fig. S4).

Brains of clinically diseased *tg*1020 mice contained multicentric PrP deposits in the stratum lacunosum-moleculare of the hippocampus, within the corpus callosum, and in the cingulum. Deposits were sometimes surrounded by vacuoles as in florid plaques of variant Creutzfeldt-Jakob disease (Fig. 1*C* and Fig. S4). Individual PrP deposits were 1 to 3 μm in diameter and often arranged in clusters of 25 to 50 particles. The density of PrP deposits varied from isolated clusters to widespread zones of diffuse aggregates (Fig. 1*C*). Spongiform change, astrogliosis, and microgliosis were also evident (Fig. 1*C*).

Peripheral nerves and skeletal muscle of RL-PrP mice developed pathologic changes similar to those reported in mice overexpressing WT or mutant PrP (12, 21). Sciatic nerves displayed "onion bulbs" indicative of cycles of active demyelination and re-myelination, as well as macrophages and Schwann cells with myelin-filled vacuoles (Fig. S5). Myofibers displayed degeneration and regeneration, varied markedly in size, and contained angular and split fibers as well as centralized nuclei (Fig. 1*D*). PrP immunohistochemistry revealed large, coarse PrP aggregates in *tg*1020 myofibers, whereas very few aggregates ($\leq$2 per muscle section) were observed in myofibers of *tga20* mice, which over-express WT *Prnp* (20) (Fig. 1*D*). PrP expression in muscle of *tg*1020 mice was higher than in WT mice, but lower than in *tga20* mice (Fig. 1*E*).

Although expression in *tga20* brain was consistently twofold higher than in *tg*1020 mice, and the PrP distribution in *tg*1020 brains was similar to that of *tga20* mice (Fig. S2), *tga20* mice did not spontaneously develop neurological disease, spongiform encephalopathy, or brain plaques during lifetimes up to 900 days.

Certain pathologies induced by PrP mutants are partially or fully suppressed by co-expression of WT-PrP (11, 22), whereas others are unaffected (23). To investigate the influence of WT-PrP on the RL-PrP disease, we bred *tg*1020 to WT mice. The clinical course of spontaneous disease and the median survival time were unaffected by WT PrP co-expression ($P = 0.27$, log-rank test; Fig. 1*B*). We also did not identify any influence of WT-PrP co-expression on the severity of spongiosis and the occurrence of PrP-immunoreactive plaques (data not shown). We then assessed the resistance of RL-PrP to proteolysis. After stringent digestion (50 or 100 μg/ml proteinase K [PK], 37 °C, 30 min), we detected PrP with a mobility corresponding to $\approx$25 kDa in a clinically sick 145-day-old *tg*1020 mouse and in a clinically healthy 60-day-old *tg*1020 mouse, whereas some young *tg*1020 mice had PK-sensitive PrP. PK digestion did not induce the typical electrophoretic mobility shift to PrP^{27-30}, suggesting that the amino terminus of RL-PrP was not cleaved (Fig. 1 *F–G*), similarly to patients with Gerstmann-Sträussler-Scheinker syndrome (24).

Prion Strain Barriers Between Mice Expressing RL-PrP or WT PrP. Local structural variations (16) imposed by the RL-PrP mutations may create transmission barriers to prion infection. We tested this possibility by intracerebrally inoculating groups ($n = 4$) of *tg*1020 and *tga20* mice with 10^4 $logLD_{50}$ of mouse-adapted Rocky Mountain Laboratory (RML) prions. Whereas *tga20* mice developed scrapie after 74 $\pm$ 6 days, *tg*1020 mice developed scrapie only after 323 $\pm$ 92 days, which decreased to 171 $\pm$ 11 days upon second passage to *tg*1020 mice (Fig. 2*A*, panel *vii*). The lower PrP^C expression levels in *tg*1020 mice does not account for the prolonged and broadened incubation time, as 10^3 $logLD_{50}$ of the same inoculum produced disease within 170 $\pm$ 12 days in WT mice, which express even lower levels of PrP^C. Therefore, expression of RL-PrP created a transmission barrier for RML prions.

Transmissibility of RL-PrP-Induced Disease. We then asked whether *tg*1020 mice spontaneously generate prions. To minimize all risks of laboratory prion contamination, *tg*1020 mice were housed in a room that had never hosted prion-infected animals, factory-new instruments were used for tissue collection, and all working surfaces for harvesting and processing tissues were protected with disposable covers. We inoculated *tg*1020 brain homogenate into *tga20* mice, as RL-PrP displays a prion conversion barrier for WT-adapted inoculum and *tga20* mice are permissive for xenogeneic strains such as chronic wasting disease (CWD) (25). After inoculation with brain homogenates derived from six terminally sick *tg*1020 mice, all 28 inoculated *tga20* mice (n = 4–6 per group, 100% attack rate) developed neurologic signs (e.g., kyphosis, hind leg clasp, paraparesis, ataxia, and pruritus) by 481 $\pm$ 59 days after inoculation (Fig. 2*A*, panels *i-vi*; Table S1). When inoculated into further *tga20* mice, brain homogenates from *tg*1020-infected *tga20* mice caused similar

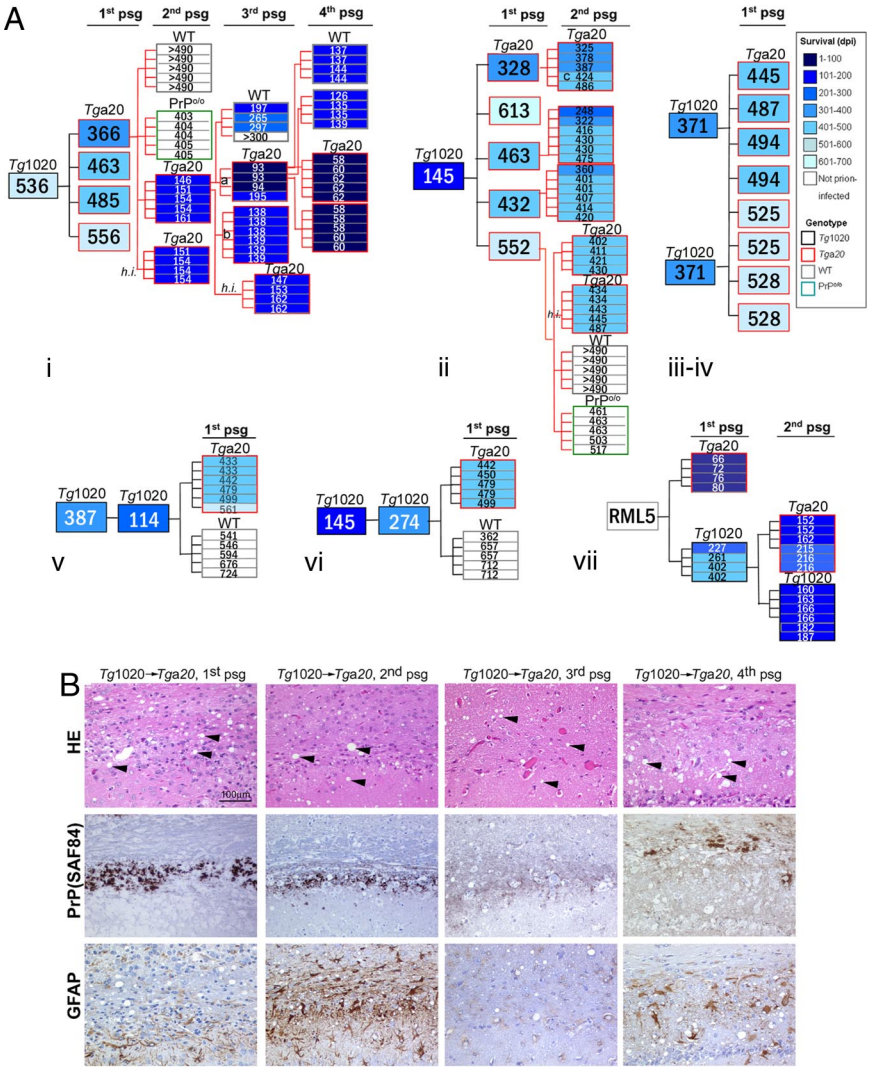

Fig. 2. *Tg*1020 prion infection transmits to *tga20* mice, but not to *Prnp*$^{o/o}$ mice. (*A*) Survival of mice inoculated with *tg*1020 brain homogenate (groups i–vi). Box outline colors denote mouse genotypes and fill colors indicate survival times as in the legend. For the first passage, only mice with incubation times more than 300 days are shown. (*h.i.* = heat inactivated.) Group vii shows RML5 passaged into *tga20* and *tg*1020 mice, and the second passage from RML-infected *tg*1020 mice. (*B*) Histopathology from transverse brain sections at the level of the hippocampus and the corpus callosum, all from group i (*A*). Sections from first to fourth passages of *tg*1020 to *tga20* mice reveal consistent spongiform changes (arrowheads). PrP deposits and astrocyte reactivity, as indicated by SAF84 and GFAP antibody staining, were apparent in all passages in *tga20* mice. PrP immunostain reveals that PrP deposit sizes decreased progressively, with granular aggregates in the fourth passage. Mock-inoculated mice did not show spongiform change or PrP staining, and gliosis was minimal (data not shown).

neurologic signs in all recipients (n = 35), but with a shorter incubation period (343 ± 122 days) suggestive of strain adaptation (Fig. 2*A*, panels *i-vi*; Table S2). Further serial passages to *tga20* led to even shorter incubation periods, and *tga20*-adapted prions were also transmissible to WT mice (Fig. 2 *A* and *B* and Fig. S6; Table S2 and Movie S1).

Brain homogenates recovered from *tg*1020-inoculated *tga20* mice were heat-inactivated at 60 °C for 20 min and inoculated into further *tga20* mice. The recipient *tga20* mice developed neurologic disease, spongiform encephalopathy, and plaques with the same incubation period (153 ± 2 days) as in the corresponding experiment without heat inactivation (153 ± 5 days). In a subsequent passage, brain homogenate was heat-inactivated at 80 °C for 25 min and was again infectious, showing that the infectious agent was highly heat-resistant (Fig. 2*A*, panel *i*).

Because *tga20* mice over-express PrP, and PrP nucleation may be concentration-dependent, we systematically tested whether serial inoculation of brain homogenate among *tga20* mice may uncover any spontaneous transmissible pathology. Brain homogenates from 30 young and old *tga20* mice (including four mice 450–900 days old) were inoculated into 16 mice. After 250 days, the latter mice were killed, and four groups of pooled brain homogenates were inoculated into 17 further *tga20* mice. After 250 more days, pooled brain homogenates from the latter mice were further inoculated into eight *tga20* mice (Fig. S7). In a further series, brain homogenate from healthy *tga20* and WT mice was inoculated into five *tga20* mice that were killed at 563 days after inoculation (Fig. S7). None of these transmission attempts resulted in neurologic disease of recipients, even after the third serial passage. We never detected spontaneous neurologic disease or PrP plaques in *tga20* mice aged up to 30 months.

Because nucleation may be time-dependent, extremely aged *tga20* mice might develop subclinical levels of prion infectivity even if clinically healthy at 900 days or older. Although no infectivity was detectable in the experiments described earlier, we again attempted transmission from brain homogenates of two 600- and 900-day-old *tga20* mice. Three of six *tga20* recipient mice developed neurologic disease and brain PrP aggregates at 422 ± 50 days post-inoculation. This suggests that low levels (≈1 ID_{50}/3 mg tissue) of prion infectivity may sporadically arise in very old *tga20* mice. The apparent occurrence of prion infectivity in some *tga20* mice is different from the prion generation in RL-PrP mice, as the former were four to six times older than the youngest *tg*1020 mice containing infectivity, and approached the natural murine lifespan, whereas the latter elicited 100% attack rates, even when inocula were prepared from 145-day-old *tg*1020 mice.

RL-PrP Prion Strain Properties. Brain homogenates from *tga20* mice infected with RL-PrP (RL → *tga20*) were subjected to PK digestion and Western blotting. PrP from first- and second-passage RL → *tga20* mice was mostly PK-sensitive (Fig. 3*A*). Weak residual PrP bands of unchanged electrophoretic mobility were identified after

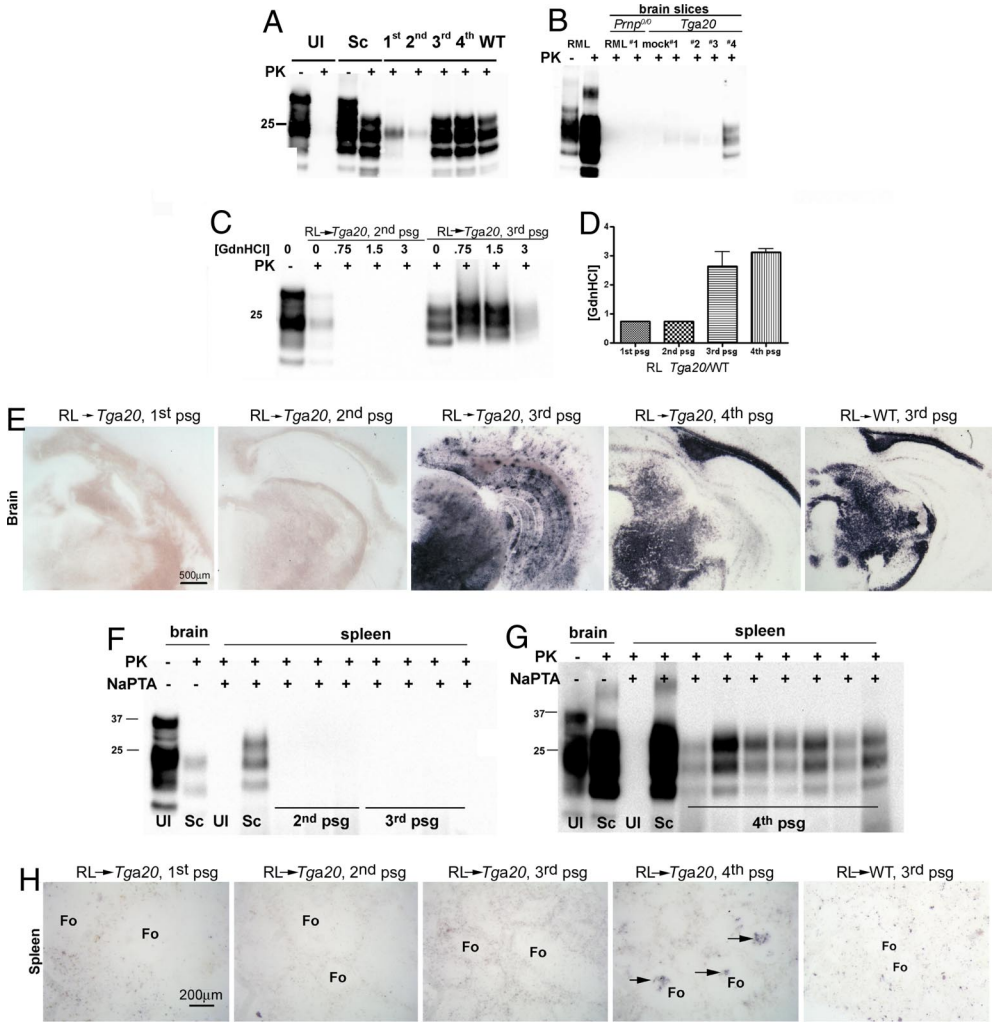

Fig. 3. Evolution of RL-PrP features over four passages of *tg*1020 → *tga20* mice. (*A*) Western blot from brain shows that the PrP switched from mostly PK-sensitive in the first and second passages to PK-resistant, with cleavage of the amino terminus in the third and fourth passages. (UI, uninfected, Sc, scrapie-infected.) (*B*) Western blot from *Prnp*$^{o/o}$ and *tga20* organotypic brain slices exposed to brain homogenate from second passage of *tg*1020 → *tga20* (n = 4 mice) shows a switch to a PK-resistant PrP in mouse 4. (*C*) Conformation stability assay indicates that PrP stability also changes between the second and third passages. (*D*) The change in the [GdnHCl], in which <25% of the original PrP signal remains, is shown for all four passages of *tg*1020 → *tga20* (n = 4–5 mice per group). No differences were identified in the first two passages. (*E*) Histoblot of brain treated with PK and stained for PrP maps the location of PK-resistant PrP. (*F*) No PK-resistant PrP was evident in the spleens in the second and third passages of *tg*1020 → *tga20*. (*G*) PrP^{Sc} was detected in all spleens tested after the fourth passage of *tg*1020 → *tga20*. (*H*) Histoblots of spleen show PrP^{Sc} deposits (arrows) only in the fourth passage of *tg*1020 → *tga20*. (Fo, follicles.)

PK digestion, similarly to the signal observed in *tg*1020 mice. However, by the third (n = 3/4) and fourth (n = 5/5) passage derived from mouse "a" (Fig. 2*A*), RL → *tga20* brain homogenates displayed abundant PK-resistant PrP$^{27–30}$ (Fig. 3*A*).

We then subjected *tg*1020 homogenates to the prion organotypic slice culture assay (26). We exposed brain slices to brain homogenates from four second-passage RL → *tga20* mice (Fig. 2, panel *ii*, from group including "c"), all of which had predominantly PK-sensitive PrP^{Sc}. Homogenates from one of four mice induced PK-resistant PrP formation in the brain slices (Fig. 3*B*), suggesting either that the switch to PK resistance is a stochastic event, or that a PK resistant strain had been progressively selected.

We quantified the resilience of PrP^{Sc} from each passage to guanidinium hydrochloride (GdnHCl) using a modified conformational stability assay (27). PrP^{Sc} from third- and fourth-passage RL → *tga20* brains displayed enhanced stability with >25% of the signal resisting exposure to 3 M GdnHCl (Fig. 3 *C* and *D*). Accordingly, PK-treated histoblots of frozen brain sections were strongly positive upon the third and fourth passages of RL → *tga20* mice and the third passage to WT mice (Fig. 3*E*).

PrP^{Sc} accumulation in lymphoid organs is a distinctive feature of some, but not all, prion strains (28). First, second, and third passage of RL → *tga20* mice did not induce PrP^{Sc} in the spleen (Figs. 3 *F* and *H*). However, fourth-passage RL → *tga20* mice accumulated splenic PrP^{Sc}, as revealed by both Western blots and histoblots (Fig. 3 *G* and *H*). The absence of lymphotropism in the third passage suggests that the strain continued to evolve between the third and the fourth passage.

Differential Staining of RL-PrP with Luminescent Conjugated Polymers (LCPs). Prion strains often differ in the affinity of PrP deposits for amyloidotropic dyes (29). This property can differentiate strains even when propagated in congenic hosts. The pathological deposits of *tg*1020 mice, RL → *tga20* mice (all four passages), and RL → WT mice were consistently negative for thioflavin T and Congo red, yet were stained by the amyloid-binding LCPs polythiophene acetic acid (PTAA; anionic) and polythiophene methyl imidazole (PTMI; cationic) (30, 31) (Fig. 4*A*). These pathological deposits were confirmed to consist of PrP by immunohistochemical staining of consecutive sections with antibody SAF84 to PrP (data not shown).

To distinguish RL-PrP from other PTAA-positive deposits, we acquired fluorescence spectra. The averaged ratios (R) of emission intensities at wavelengths $R_{532:641}$ and $R_{532:Emax}$ (E_{max}, emission maximum) recorded for individual animals allowed for unequivocal discrimination between RL → *tga20* and aggregates of other strains (Fig. 4*B*). The $R_{532:641}$ values of PTAA-stained *tg*1020 and RL → *tga20* plaques were nearly identical (analysis of variance [ANOVA], $P < 0.05$), supporting the notion that *tga20* aggregates originated from the RL prion strain. In contrast, PTAA spectra from the RL-PrP aggregates differed significantly from those of other mouse-adapted prion strains, and PTAA did not detect bovine spongiform encephalopathy or RML aggregates (Fig. 4 *C* and *D*; ANOVA, $P > 0.05$). Therefore, the morphological characteristics,

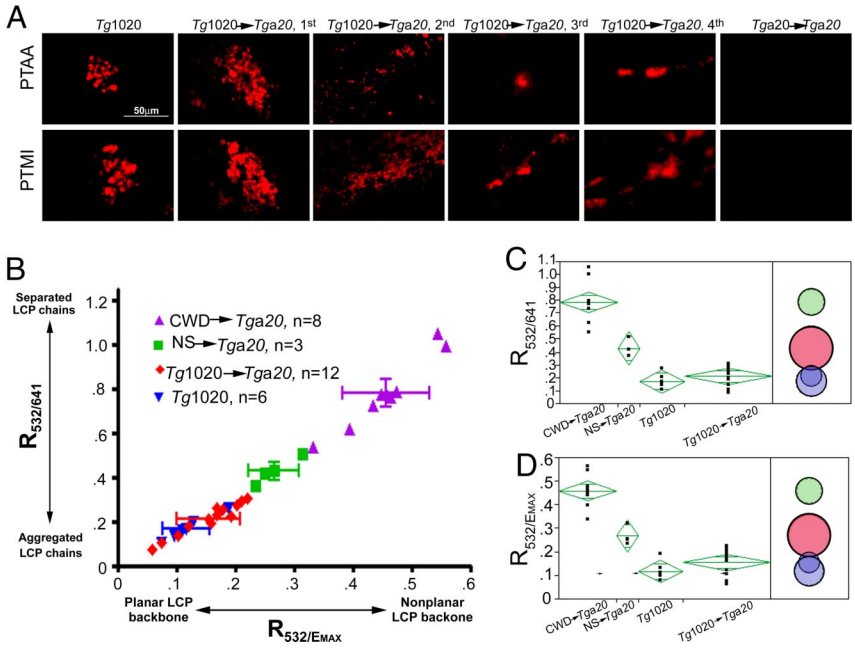

Fig. 4. LCP fluoroscopy distinguishes RL-PrP from other mouse prion strains. (*A*) Tg1020 and *Tg*1020 → *Tga20* PrP aggregates in brain tissue were stained using anionic and cationic conjugated poly-electrolyte probes (PTAA and PTMI, respectively). Spectral intensity measurements were recorded from PTAA-stained sections at 10-nm intervals between 500 and 750 nm. Spectral unmixing visualizes the pixels with similar spectral profiles. (*B*) Intensity ratios of fluorescence, $R_{532/641}$, and $R_{532/Emax}$, from PTAA-stained plaques in individual CWD → *tga20*-, NS → *tga20*-, and *tg*1020 → *tga20*-infected mice, as well as un-inoculated *tg*1020 mice. (NS, natural sheep scrapie.) (*C* and *D*) Statistical analysis was performed using ANOVA followed by Tukey-Kramer honestly significantly different (HSD) test for the spectral ratios, $R_{532/641}$, and $R_{532/Emax}$ (general α level of 0.05). The green diamonds illustrate the sample means and the corresponding 95% CIs (one black dot per animal). Lines across each diamond represent group means. The vertical span of each diamond represents the 95% CI for each group. Overlap marks are drawn above and below the group mean. Comparison circle plots are shown for Tukey-Kramer HSD test (*Right*). Circles for means that are significantly different do not intersect, or intersect so slightly that the outside angle of intersection is <90°.

the tinctorial properties of RL-PrP aggregates, and the emission spectra are similar in *tg*1020 mice and across four serial passages to *tga20* and WT mice, and profoundly differ from all other murine PrP deposits in our laboratory, including those induced in mice by CWD, bovine spongiform encephalopathy, natural sheep scrapie, and RML prions.

Discussion

We report that the alteration of two codons in the PrP reading frame, whose conformational consequences on the encoded protein are understood in atomic detail (16), induces a progressive neurologic disease in transgenic mice. Although clinical signs arose stochastically and often late in life, the penetrance of the disease was 100%. The RL-PrP disease, unlike the syndromes associated with overexpression of WT PrP (21), was caused by the loop mutations, given that *tga20* mice that expressed >2-fold higher PrP protein levels than RL-PrP mice did not develop spontaneous PrP plaques, histological signs, or clinical prion disease.

Several internally deleted PrP variants cause neurodegeneration, which is suppressed by co-expression of WT PrP (11, 22, 32). In contrast, the concomitant presence of PrP did not influence any of the clinical and histological parameters of the RL-PrP disease. Therefore, the RL-PrP disease arises by fundamentally different mechanisms than the aforementioned syndromes.

Conversely, the spongiform degeneration, the conspicuous PrP plaques, and the deposition of partially PK-resistant PrP in the brain of *tg*1020 mice were suggestive of a bona fide prion disease. This conjecture was substantiated by the transmissibility of the RL-PrP disease to young *tga20* and, after adaptation, to WT mice, but not to *Prnp*$^{o/o}$ mice. Disease transmission occurred even after extensive heat-treatment of *tg*1020 brain homogenate, virtually ruling out any conventional infectious agent.

The failure to directly transmit disease from RL-PrP to WT mice, and the highly variable incubation periods of first-passage RL-PrP in *tga20* mice, may point to a transmission barrier imposed by the 170N and 174T substitutions in mPrP. This barrier appeared to be bidirectional, as *tg*1020 mice experienced long, highly variable incubation periods upon inoculation with RML mouse prions. The incubation time and its variability decreased by ≈50% on second passage in *tg*1020 mice, as would be expected from strain adaptation (25, 33, 34).

Progressive alterations in the disease phenotype occurred over the course of four RL-PrP passages in *tga20* mice, such as shortening of incubation periods, a shift from plaque-like to synaptic-diffuse cerebral PrP deposits, progressively increased resistance of PrP to PK, and, by the fourth passage, acquisition of lymphotropism. These changes suggest that the conformation and/or the size of the PrP aggregates underwent gradual changes. Alternatively, the original seeds in RL-PrP mice may be heterogeneous and propagate at different rates, with the fittest sub-strains being gradually selected and eventually becoming dominant. However, the evolution of biochemical properties and pathological features was not accompanied by shifts in PTAA emission spectra, indicating that certain core properties of RL-PrP prions were stable over at least four passages. PTAA interacts anisotropically with amyloid, and its emission spectrum reports on the structure of PrP^{Sc} aggregates (29). The stability of PTAA spectra suggests that an aspect of the structure of RL-PrP aggregates is faithfully propagated onto WT PrP aggregates over many generations. Conversely, the strain adaptation phenomena described may result from interaction with ancillary, non-PrP constituents.

After several passages into *tga20* mice, RL-PrP acquired PK resistance and proteolysis patterns similar to those of the murine laboratory prion strain, RML. These phenomena are unlikely to stem from contamination or cross-infection with RML prions. First, RML-infected brains are PTAA-negative (29), whereas RL-PrP aggregates of *tg*1020 mice and all passages therefrom were consistently PTAA-positive. Second, RL → *tga20* PrP was PK-resistant by the third passage, yet was not lymphotropic, whereas RML is heavily lymphotropic (35). Third, the clinical disease and incubation period varied vastly within and between groups of mice inoculated with two second-passage RL → *tga20* mice, whereas the incubation period of RML is highly consistent, with <5 days variation within a group. Fourth, brain histoblots of third-passage RL → *tga20* revealed large, patchy aggregates, unlike the diffuse stains of RML.

What is the mechanism initiating RL-PrP prion formation? The loop region of PrP contains several glutamine and asparagine residues, which are common in amyloidogenic proteins and may act as "hot spots" in protein aggregation (36). In amyloid aggregates of short fibril-forming polypeptides, glutamines and asparagines can form multiple intermolecular hydrogen bonds (i.e., "steric zippers") (37). NMR spectroscopy and molecular

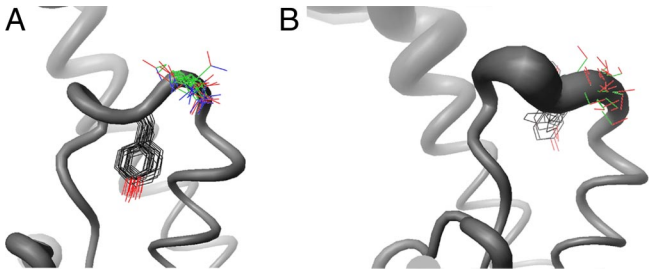

Fig. 5. The RL-PrP and WT-mPrP loop regions. (*A*) The 169Y and 170N side chains are quite precisely defined in the NMR structure of RL-PrP (16), and the side chain of 170N (green) protrudes from the core of the molecule. (*B*) The 169Y and 170S side chains in the NMR structure of WT-mPrP are disordered. The different features of the side chains of residues 169 and 170 in the two proteins are also predicted by molecular dynamic simulations (38).

dynamics simulations indicate that the N170 residue protrudes highly directionally from PrP^C, whereas S170 is disordered (16, 38). Hence the N170 asparagine side chain might engage in long-range intermolecular hydrogen bonds with complementary sequences and initiate steric zippers (Fig. 5). Alternative mechanisms of amyloidogenesis are equally conceivable, including the disruption of interactions between the loop region and hypothetical anti-amyloidogenic chaperones.

If the RL substitutions are pathogenic for mice, why was no spontaneous prion disease observed in transgenic mice overexpressing cervid PrP^C (39, 40)? In addition to the two loop residues, cervid and mouse PrP^C differ at 11 further positions within their globular domains, seven of which are located near the C-terminal end of the α3 helix. This site is thought to be important for species-specific molecular interactions in TSE transmission. Therefore, some of these substitutions may even have evolved to counteract enhanced aggregation tendencies. A comparison of the three-dimensional structures of elk PrP with murine PrP shows that the orientation of the α3 helix is closely similar in the two proteins (16). However, a change in the polarity and/or charge of specific amino acid side chains in this area might nonetheless modify the specificity of this surface area for intermolecular interactions. In view of these results, it will be interesting to assess the impact wrought by the structural features of the rigid loop onto the enigmatic pathogenesis and transmission barriers of cervid CWD. Further studies may help clarify the significance of the β2—α2 loop region on prion disease development and species barriers.

Materials and Methods

Refer to *SI Text* for detailed materials and methods and for a description of the transgene construct and mouse characterization.

Prion Inoculations. For detailed methods, refer to *SI Text*. Briefly, mice were intracerebrally inoculated into the left parietal cortex with 30 μl of a 5% brain homogenate from an un-inoculated *tg*1020 mouse, an un-inoculated *tga20* mouse, and subsequently from *tga20* mice infected with RL-PrP prions. Brains from terminal mice were collected using new instruments on new surface covers.

Histopathology and Immunohistochemical Stains. For detailed methods, refer to *SI Text*. Briefly, 2-μm-thick sections were cut onto positively charged silanized glass slides and stained with hematoxylin and eosin, or immunostained using antibodies for PrP (SAF84), astrocytes (GFAP), or microglia (Iba1).

ACKNOWLEDGMENTS. We thank Frank Baumann, Jens Pahnke, Gino Miele, Sei-ichi Yusa, Kirsten Mertz, Amedeo Caflisch, and Pietro Alfarano for discussions; Petri Vilkman, Marianne König, and the animal care staff for technical support; and Michel Mittelbronn and Burkhard Seifert for help with statistics. This study was supported by the European Union TSEUR collaborative research project (A.A.) and Understanding Protein Misfolding and Aggregation by NMR program (K.W.), the Swiss National Science Foundation (A.A.), the National Competence Centers for Research on Neural Plasticity and Repair (A.A.) and on Structural Biology (K.W.), National Institutes of Health grants K08-AI01802 and 5R21NS055116 (to C.J.S.), the Foundation for Research at the University of Zürich (C.J.S.), the US National Prion Research Program (C.J.S. and A.A.), the Knut and Alice Wallenberg Foundation (K.P.R.N.), the Max-Clöetta and Bonizzi-Theler Foundations (M.H.), Stammbach Foundation (A.A.), and ETH Zürich (K.W.).

1. Prusiner SB (1982) Novel proteinaceous infectious particles cause scrapie. *Science* 216:136–144.
2. Büeler HR, *et al.* (1993) Mice devoid of PrP are resistant to scrapie. *Cell* 73:1339–1347.
3. Hsiao K, *et al.* (1989) Linkage of a prion protein missense variant to Gerstmann-Sträussler syndrome. *Nature* 338:342–345.
4. Goldfarb LG, *et al.* (1992) Fatal familial insomnia and familial Creutzfeldt-Jakob disease: disease phenotype determined by a DNA polymorphism. *Science* 258:806–808.
5. Medori R, *et al.* (1992) Fatal familial insomnia, a prion disease with a mutation at codon 178 of the prion protein gene. *N Engl J Med* 326:444–449.
6. Manson JC, *et al.* (1999) A single amino acid alteration (101L) introduced into murine PrP dramatically alters incubation time of transmissible spongiform encephalopathy. *EMBO J* 18:6855–6864.
7. Tateishi J, *et al.* (1995) First experimental transmission of fatal familiar insomnia. *Nature* 376:434–435.
8. Hsiao KK, *et al.* (1990) Spontaneous neurodegeneration in transgenic mice with mutant prion protein. *Science* 250:1587–1590.
9. Chiesa R, Piccardo P, Ghetti B, Harris DA (1998) Neurological illness in transgenic mice expressing a prion protein with an insertional mutation. *Neuron* 21:1339–1351.
10. Hsiao KK, *et al.* (1994) Serial transmission in rodents of neurodegeneration from transgenic mice expressing mutant prion protein. *Proc Natl Acad Sci USA* 91:9126–9130.
11. Shmerling D, *et al.* (1998) Expression of amino-terminally truncated PrP in the mouse leading to ataxia and specific cerebellar lesions. *Cell* 93:203–214.
12. Telling GC, *et al.* (1996) Interactions between wild-type and mutant prion proteins modulate neurodegeneration in transgenic mice. *Genes Dev* 10:1736–1750.
13. Nazor KE, *et al.* (2005) Immunodetection of disease-associated mutant PrP, which accelerates disease in GSS transgenic mice. *EMBO J* 24:2472–2480.
14. Riek R, *et al.* (1996) NMR structure of the mouse prion protein domain PrP(121–231). *Nature* 382:180–182.
15. Lysek DA, *et al.* (2005) Prion protein NMR structures of cats, dogs, pigs, and sheep. *Proc Natl Acad Sci USA* 102:640–645.
16. Gossert AD, Bonjour S, Lysek DA, Fiorito F, Wüthrich K (2005) Prion protein NMR structures of elk and of mouse/elk hybrids. *Proc Natl Acad Sci USA* 102:646–650.
17. Lopez Garcia F, Zahn R, Riek R, Wüthrich K (2000) NMR structure of the bovine prion protein. *Proc Natl Acad Sci USA* 97:8334–8339.
18. Zahn R, *et al.* (2000) NMR solution structure of the human prion protein. *Proc Natl Acad Sci USA* 97:145–150.
19. Schätzl HM, Da Costa M, Taylor L, Cohen FE, Prusiner SB (1995) Prion protein gene variation among primates. *J Mol Biol* 245:362–374.
20. Fischer M, *et al.* (1996) Prion protein (PrP) with amino-proximal deletions restoring susceptibility of PrP knockout mice to scrapie. *EMBO J* 15:1255–1264.
21. Westaway D, *et al.* (1994) Degeneration of skeletal muscle, peripheral nerves, and the central nervous system in transgenic mice overexpressing wild-type prion proteins. *Cell* 76:117–129.
22. Baumann F, *et al.* (2007) Lethal recessive myelin toxicity of prion protein lacking its central domain. *EMBO J* 26:538–547.
23. Chiesa R, *et al.* (2000) Accumulation of protease-resistant prion protein (PrP) and apoptosis of cerebellar granule cells in transgenic mice expressing a PrP insertional mutation. *Proc Natl Acad Sci USA* 97:5574–5579.
24. Colucci M, *et al.* (2006) Gerstmann-Sträussler-Scheinker: a new phenotype with 'curly' PrP deposits. *J Neuropathol Exp Neurol* 65:642–651.
25. Sigurdson CJ, *et al.* (2006) Strain fidelity of chronic wasting disease upon murine adaptation. *J Virol* 80:12303–12311.
26. Falsig J, *et al.* (2008) A versatile prion replication assay in organotypic brain slices. *Nat Neurosci* 11:109–117.
27. Peretz D, *et al.* (2001) Strain-specified relative conformational stability of the scrapie prion protein. *Protein Sci* 10:854–863.
28. Aguzzi A, Sigurdson CJ (2004) Antiprion immunotherapy: to suppress or to stimulate? *Nat Rev Immunol* 4:725–736.
29. Sigurdson CJ, *et al.* (2007) Prion strain discrimination using luminescent conjugated polymers. *Nat Methods* 4:1023–1030.
30. Ho H-A, Boissinot M, Bergeron MG, Corbeil G, Dore K, Boudreau D, Leclerc M (2002) Colorimetric and fluorometric detection of nucleic acids using cationic polythiophene derivatives. *Angew Chem Int Ed Engl* 41:1548–1551.
31. Nilsson KPR, *et al.* (2006) Conjugated polyelectrolytes-conformation-sensitive optical probes for staining and characterization of amyloid deposits. *Chembiochem* 7:1096–1104.
32. Li A, *et al.* (2007) Neonatal lethality in transgenic mice expressing prion protein with a deletion of residues 105–125. *EMBO J* 26:548–558.
33. Bartz JC, Bessen RA, McKenzie D, Marsh RF, Aiken JM (2000) Adaptation and selection of prion protein strain conformations following interspecies transmission of transmissible mink encephalopathy. *J Virol* 74:5542–5547.
34. Race R, *et al.* (2002) Subclinical Scrapie Infection in a Resistant Species: Persistence, Replication, and Adaptation of Infectivity during Four Passages. *J Infect Dis* 186(suppl 2):S166–S170.
35. Aguzzi A (2003) Prions and the immune system: a journey through gut, spleen, and nerves. *Adv Immunol* 81:123–171.
36. Balbirnie M, Grothe R, Eisenberg DS (2001) An amyloid-forming peptide from the yeast prion Sup35 reveals a dehydrated beta -sheet structure for amyloid. *Proc Natl Acad Sci USA* 98:2375–2380.
37. Sawaya MR, *et al.* (2007) Atomic structures of amyloid cross-beta spines reveal varied steric zippers. *Nature* 447:453–457.
38. Gorfe AA, Caflisch A (2007) Ser170 controls the conformational multiplicity of the loop 166–175 in prion proteins: implication for conversion and species barrier. *FASEB J* 21:3279–3287.
39. Browning SR, *et al.* (2004) Transmission of prions from mule deer and elk with chronic wasting disease to transgenic mice expressing cervid PrP. *J Virol* 78:13345–13350.
40. Tamguney G, *et al.* (2006) Transmission of elk and deer prions to transgenic mice. *J Virol* 80:9104–9114.
41. Forster MJ, Morris P, Sohal RS (2003) Genotype and age influence the effect of caloric intake on mortality in mice. *FASEB J* 17:690–692.